Nationaal Lucht- en Ruimtevaartlaboratorium
National Aerospace Laboratory NLR

NLR-TP-2004-165

Experimental techniques for identification and characterisation of noise sources

P. Sijtsma

This report has been based on a paper presented at VKI Lecture Series "Advances in Aeronautics & Applications", at Rhode-Saint-Genèse, Belgium on 15-19 March 2004 and will also be published in VKI Lecture Series "Advances in Aeronautics & Applications".

Customer:	National Aerospace Laboratory NLR
Working Plan number:	AV.1.C.1
Owner:	National Aerospace Laboratory NLR
Division:	Aerospace Vehicles
Distribution:	Unlimited
Classification title:	Unclassified
	April 2004

Approved by author:	Approved by project manager:	Approved by project managing department:
14/5/04	4/6/04	15/6

Summary

An introduction is given of phased array beamforming with microphone arrays. Beamforming is considered both in the time-domain and in the frequency-domain. Conventional beamforming techniques are treated, but also more advanced techniques. Special attention is paid to the localisation of moving sources. Applications are shown of wind tunnel measurements and aircraft fly-over measurements.

Contents

(47 pages in total)

Nomenclature

Symbols

A	source auto-power
$\overline{A}$	estimated source auto-power
$\overline{A}_h$	source auto-power estimate of measurements
$\overline{A}_{\max}$	peak level of $\overline{A}_h$
$\overline{A}_{s,h}$	source auto-power estimate of simulated point source
$\overline{A}_{s,\max}$	peak level of $\overline{A}_{s,h}$
$\tilde{A}_h$	see Eq. (86)
$\tilde{A}_{s,h}$	see Eq. (87)
a	complex pressure amplitude at source
$\overline{a}$	estimated complex source amplitude
$\mathbf{C}$	cross-power matrix
C_{mn}	microphone cross-power
C_{nn}	microphone auto-power
c	speed of sound
d_{mn}	see Eq. (59)
D	array diameter
$\mathbf{E}$	diagonal matrix with eigenvalues of $\mathbf{C}$
e_λ	eigenvalue of $\mathbf{C}$
F	transfer function from moving source in $\vec{\xi}(t)$ to receiver in $\vec{x}$
F_n	transfer function from $\vec{\xi}(t)$ to n-th microphone (cf. Eqs. (102) and (103))
f	frequency
$f_{\max}$	maximum frequency
f_{sam}	sample frequency
G	Green's function
G_{mn}	cross-spectral density function
g	steering function
$\mathbf{g}$	steering vector
H	number of grid points
h	grid index
i	imaginary unit
j	frequency index
J	functional to minimise
J_0	zero-th order Bessel function of the first kind
K	number of samples during one time period (block size)
k	sample index

L	number of eigenvalues
$\vec{M}$	Mach number vector of uniform flow
m	microphone index
N	number of microphones
n	microphone index
P	integrated source power
P_s	source power of simulated monopole
$\mathbf{p}$	pressure vector
$p(\vec{x})$	complex acoustic pressure amplitude
p_n	complex pressure amplitude at n-th microphone
$\mathbf{Q}$	matrix with eigenvectors of $\mathbf{C}$
q	see Eq. (14)
$R_{mn}(t)$	cross-correlation function
S	set of pairs (m,n) for which C_{mn} is not discarded
T	time period ($T = K\Delta t$)
t	time
t_1	see Eq. (92)
t_n	reception time at n-th microphone
$\vec{U}$	uniform flow speed
u_k	weight factor for FFT window
W	aperture smoothing function
$\mathbf{w}$	weight vector for beamforming
$\vec{x}$	cartesion position vector
$\vec{x}_1$	see Eq. (92)
$\vec{x}_n$	position of n-th microphone
x_n	x-component of position of n-th microphone
Y	distance between source and array
y_n	y-component of position of n-th microphone
Z	dynamic range for source power integration without auto-powers
z_n	z-component of position of n-th microphone

Greek

$\vec{\alpha}$	wave number vector
$\alpha_{\min}$	minimum value for $\|\vec{\alpha}\|$
$\alpha_{\max}$	maximum value for $\|\vec{\alpha}\|$
α_x	x-component of $\vec{\alpha}$
α_y	y-component of $\vec{\alpha}$
β	see Eq. (39)

γ	auxiliary function in Eq. (98)
Δt	sample interval ($\Delta t = 1/f_{\text{sam}}$)
Δt_e	emission time delay
$\Delta t_{e,n}$	microphone-dependent emission time delay
δ	Dirac delta function
$\varepsilon_n(t)$	noise on n-th microphone
$\chi(\vec{x},t)$	acoustic pressure field
$\chi_n(t)$	fluctuating pressure measured by n-th microphone
$\chi_{n,k}$	sampled acoustic pressure measured by n-th microphone
λ	eigenvalue index
μ	control parameter (Robust Adaptive Beamforming)
ν	average index
$\sigma(t)$	emitted source signal
$\bar{\sigma}(t)$	estimated source signal
τ	integration parameter (time)
τ_e	emission time
$\vec{\xi}$	(potential) source position
$\vec{\xi}_0$	(unknown) source position

Operator

∇	Nabla operator: $\nabla = (\partial/\partial x, \partial/\partial y, \partial/\partial z)$

Superscript

$(\cdot)^*$	complex conjugate (transpose)

Subscript

$(\cdot)_a$	induced by acoustic pressure
$(\cdot)_{CB}$	for Conventional Beamforming
$(\cdot)_j$	for j-th frequency
$(\cdot)_h$	for h-th grid point
$(\cdot)_k$	for k-th sample
$(\cdot)_l$	for l-th source/principal component
$(\cdot)_m$	for m-th microphone
$(\cdot)_n$	for n-th microphone
$(\cdot)_s$	corresponding to simulated point source
$(\cdot)_w$	induced by wind
$(\cdot)_\lambda$	for λ-th eigenvalue
$(\cdot)_\nu$	after ν averages

Abbreviations

DFT	Discrete Fourier Transform
DNW	German-Dutch Wind Tunnels
FFT	Fast Fourier Transform
LST	Low-speed Wind Tunnel
LLF	Large Low-speed Facility
WNC	White Noise gain Constraint

This page is intentionally left blank.

1 Introduction

There is a continuous pressure, driven by public opinion, to reduce noise from industry, cars, trains, aircraft, wind turbines, etc. In order to reduce noise, it is important to understand the noise generation process. Sometimes, noise sources are well known, and solutions are evident (e.g. insulation). In many cases, however, the noise origin is not obvious. Even the actual position of the (loudest) noise source may be unknown. Knowledge of the source position is, of course, the first step towards noise reduction.

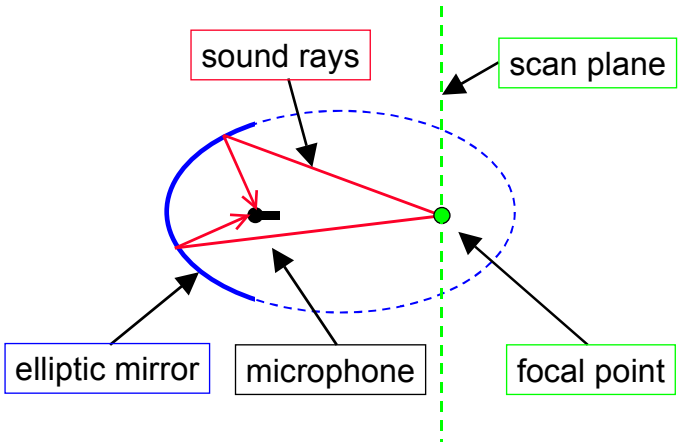

Figure 1: Principle of elliptic mirror.

A possibility to locate acoustic sources is by means of an elliptic “acoustic” mirror (Refs. 1,2). The concept of an acoustic mirror is based on the fact that acoustic rays emerging from one focal point of the ellipse converge to the other focal point (see Figure 1). A microphone is placed in the focal point close to the mirror, while the other focal point scans through a surface of possible noise sources. This scanning can be done by traversing the mirror or by moving the studied object. An example of a recent set-up with an acoustic mirror in the DNW-LLF is shown in Figure 2.

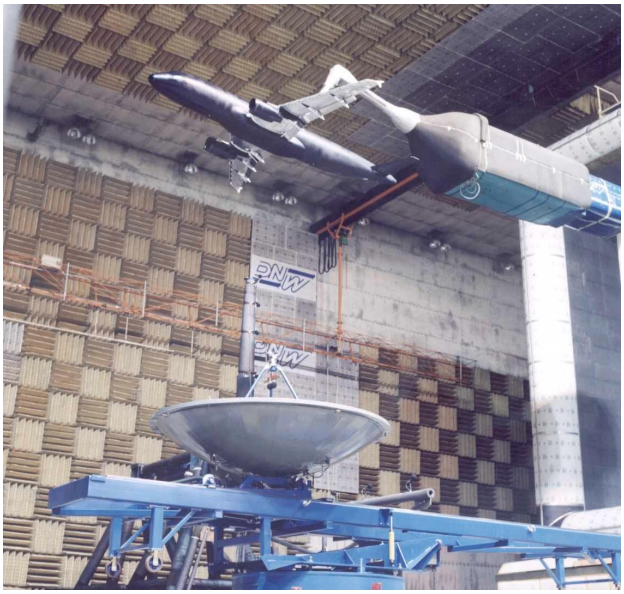

Figure 2 Set-up with acoustic mirror in DNW-LLF

By scanning with acoustic mirrors, source locations can by found at high accuracy. Sources close to each other can be separated well. The range of frequencies to which acoustic mirrors can be applied is large. Furthermore, background noise is filtered out effectively. The main drawback of acoustic mirrors is the long time that is needed for measurements. The mirror (or the studied object) has to be moved for each scan point. Consequently, measurements with acoustic mirrors are expensive, especially in large wind tunnels.

Since the 1970's (Refs. 3, 4) developments are ongoing on the alternative for the acoustic mirror: the "acoustic array". An acoustic array is a set of microphones, of which the signals are combined in such a way that sound from a specified focal point is amplified and sound from other directions is attenuated. This signal combination is done through appropriately delaying and summing the individual microphone signals. In the frequency-domain this comes down to applying microphone-dependent phase shifts. Thus, the acoustic array is a special type of "phased array", also applied in seismology, astronomy and underwater acoustics (sonar). The advantage of acoustic arrays is that only short measurement time is needed, because the process of scanning through possible source locations is performed afterwards.

Until recently, the acoustic array could not outperform the acoustic mirror in spatial resolution, frequency range and signal/noise ratio. The main reason for this was the limited capacity of data-acquisition systems (data-loggers), so that the number of microphones had to be limited. Nowadays, however, the increasing capacity of computers and data acquisition systems have enabled the use of large numbers of microphones, long acquisition times and high sample frequencies (Ref. 5). Thus, the traditional drawbacks of microphone arrays compared to acoustic

mirrors, namely lower resolution and lower signal/noise ratio, are vanishing. What remains is the great advantage of arrays, that is, the short time needed for measurements.

In addition, microphone arrays offer the opportunity to locate sources on moving objects. This application, which is relatively new, has been implemented on objects in steady, rectilinear motion, like trains passing by (Refs. 6, 7) and airplanes flying over (Refs. 8, 9). The technique of de-Dopplerisation (Refs. 10, 11) was applied to recalculate, from the microphone signals, the source signals in the moving frame. In reference 12, it was shown that acoustic source location by a microphone array is, in principle, possible on objects in any given subsonic motion. Besides, it was made clear that the presence of a uniform flow does not form any limitation. Therefore, source location measurements on arbitrarily moving objects in wind tunnels are feasible too. In reference 12, applications were shown to rotating sources like rotating whistles and broadband sources on wind turbine and helicopter blades.

The technique of locating sources using phased arrays is called “beamforming”. Basically, it is an algorithm, applied to each scan point individually, which amplifies the sound from the scan point and attenuates the sound from other directions. The source is then identified as the scan point from which the beamforming algorithm yields maximum output. There are a large number of beamforming techniques available (Ref. 13), e.g. developed for astronomy. Many of those, however, do not work very well for acoustics. Here, we limit ourselves to those techniques that are able to cope with the specific difficulties of acoustic measurements, such as background noise, coherence loss, errors in the transfer model, and calibration uncertainties.

In the following, we will start with beamforming in the time-domain, because time-domain beamforming gives the most insight. However, the major part of this treatise is devoted to frequency-domain beamforming, because that is in many cases the most convenient. In the final chapter, when moving sources are considered, we will inevitably return to time-domain beamforming.

At the end of this introduction it is remarked that, besides beamforming, a completely different technique exists of identifying noise sources with microphone arrays: “Near-field Acoustic Holography”. This technique is based on the principle that, if the acoustic pressure is known on a given closed surface that does not enclose acoustic sources, the acoustic pressure can be calculated everywhere inside this surface. Near-field Acoustic Holography is not considered here, but it is treated very clearly in reference 14.

2 Time-domain beamforming

2.1 Preliminaries

Consider a set of N microphones, located in $\vec{x}_n = (x_n, y_n, z_n)$, where n runs from 1 to N. At these positions, the local pressure fluctuations:

$$\chi_n(t) = \chi(\vec{x}_n, t) \tag{1}$$

are recorded. It is assumed that a point source with uniform directivity (monopole) exists at an unknown location $\vec{\xi}_0$ on a scan surface. The associated acoustic pressure field is

$$\chi(\vec{x}, t) = \frac{\sigma\left(t - \Delta t_e\right)}{4\pi \left\| \vec{x} - \vec{\xi}_0 \right\|}, \tag{2}$$

where $\sigma(t)$ is the emitted source signal and Δt_e is the emission time delay:

$$\Delta t_e = \frac{\left\| \vec{x} - \vec{\xi}_0 \right\|}{c}, \tag{3}$$

in which c is the speed of sound.

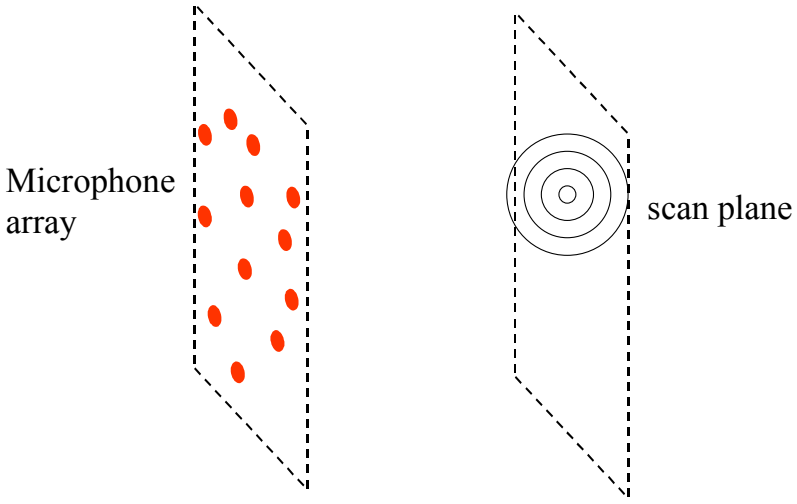

Figure 3 Microphone array and scan plane

A beamforming algorithm is a calculation procedure that uses microphone signals and potential source locations as input. With a beamforming algorithm a “scan” can be made through a set of potential source locations, usually on a plane surface (Figure 3). The algorithm should be such

that maximum output is obtained when the potential source location coincides with the actual source location.

2.2 Delay and Sum

An obvious choice for a beamforming algorithm on a potential source location (scan point) $\vec{\xi}$, is the so-called "Delay and Sum" algorithm, in which each microphone signal is multiplied with the distance to the potential source, and time-shifted accordingly:

$$\bar{\sigma}(t) = \frac{1}{N}\sum_{n=1}^{N} 4\pi \left\| \vec{x}_n - \vec{\xi} \right\| \chi_n(t + \Delta t_{e,n}) . \tag{4}$$

Herein, $\bar{\sigma}(t)$ is the "estimated source signal" and $\Delta t_{e,n}$ is the microphone-dependent emission time delay:

$$\Delta t_{e,n} = \frac{\left\| \vec{x}_n - \vec{\xi} \right\|}{c} . \tag{5}$$

Substituting the actual (but unknown) pressure field (2) into (4), we obtain:

$$\bar{\sigma}(t) = \frac{1}{N}\sum_{n=1}^{N} \frac{\left\| \vec{x}_n - \vec{\xi} \right\|}{\left\| \vec{x}_n - \vec{\xi}_0 \right\|} \sigma\left(t + \frac{1}{c}\left\{ \left\| \vec{x}_n - \vec{\xi} \right\| - \left\| \vec{x}_n - \vec{\xi}_0 \right\| \right\} \right). \tag{6}$$

Clearly, when $\vec{\xi}$ coincides with the actual source location $\vec{\xi}_0$, we obtain $\bar{\sigma}(t) = \sigma(t)$. For other potential source locations ($\vec{\xi} \neq \vec{\xi}_0$), we will usually find $\left|\bar{\sigma}(t)\right| < \left|\sigma(t)\right|$.

2.3 Least Squares

An alternative for Delay and Sum Beamforming is Least Squares Beamforming. Herein, the source signal is estimated by minimising the following expression:

$$J = \sum_{n=1}^{N} \left| \chi_n(t + \Delta t_{e,n}) - \frac{\bar{\sigma}(t)}{4\pi \left\| \vec{x}_n - \vec{\xi} \right\|} \right|^2 . \tag{7}$$

Hence, the difference is minimised between the actual microphone signal and the microphone signal that would be induced by a potential source in $\vec{\xi}$. The solution of the minimisation problem is:

$$\bar{\sigma}(t)=\sum_{n=1}^{N}\frac{\chi_n(t+\Delta t_{e,n})}{4\pi\left\|\vec{x}_n-\vec{\xi}\right\|}\Bigg/\sum_{n=1}^{N}\frac{1}{\left(4\pi\left\|\vec{x}_n-\vec{\xi}\right\|\right)^2}. \tag{8}$$

Substituting the actual pressure (2) into (8), we obtain

$$\bar{\sigma}(t)=\sum_{n=1}^{N}\frac{\sigma\left(t+\frac{1}{c}\left(\left\|\vec{x}_n-\vec{\xi}\right\|-\left\|\vec{x}_n-\vec{\xi}_0\right\|\right)\right)}{\left(4\pi\left\|\vec{x}_n-\vec{\xi}\right\|\right)\left(4\pi\left\|\vec{x}_n-\vec{\xi}_0\right\|\right)}\Bigg/\sum_{n=1}^{N}\frac{1}{\left(4\pi\left\|\vec{x}_n-\vec{\xi}\right\|\right)^2}. \tag{9}$$

Again, for $\vec{\xi}=\vec{\xi}_0$ we find $\bar{\sigma}(t)=\sigma(t)$, and for $\vec{\xi}\neq\vec{\xi}_0$ we expect $\left|\bar{\sigma}(t)\right|<\left|\sigma(t)\right|$.

The main difference between Delay and Sum Beamforming (4) and Least Squares Beamforming (8) is the relative weight of the microphone signals. For Delay and Sum, the microphone signals are multiplied with a factor proportional to the distance $\left\|\vec{x}_n-\xi\right\|$. For Least Squares, that factor is *inverse* proportional to the distance. When the microphone signals contain noise, Least Squares is preferable to Delay and Sum, because Delay and Sum multiplies the noise disproportionately for microphones that are relatively far away from the source.

2.4 Limitation of time-domain approach

An important aspect of beamforming techniques is the spatial resolution, i.e., how well can the actual source location be recognised from the results of the scan. In other words, how rapidly does the beamforming output $\bar{\sigma}(t)$ vanish for increasing distance between assumed source location $\vec{\xi}$ and actual source location $\vec{\xi}_0$. However, it is difficult to quantify the right hand side of Eq. (9) when $\vec{\xi}\neq\vec{\xi}_0$. In that case, in (9) a number of σ-values with *n*-dependent arguments has to be summed. The outcome of this summation can not be predicted without knowledge of the characteristics (auto-correlation) of the source signal $\sigma(t)$.

It is more convenient to study aspects like spatial resolution in the frequency-domain. This can be seen, for instance, by Fourier transforming Eq. (9):

$$\bar{a}(f)=a(f)\sum_{n=1}^{N}\frac{\exp\left(\frac{2\pi i f}{c}\left(\left\|\vec{x}_n-\vec{\xi}\right\|-\left\|\vec{x}_n-\vec{\xi}_0\right\|\right)\right)}{\left(4\pi\left\|\vec{x}_n-\vec{\xi}\right\|\right)\left(4\pi\left\|\vec{x}_n-\vec{\xi}_0\right\|\right)}\Bigg/\sum_{n=1}^{N}\frac{1}{\left(4\pi\left\|\vec{x}_n-\vec{\xi}\right\|\right)^2}, \tag{10}$$

where a and $\bar{a}$ are the Fourier transforms of σ and $\bar{\sigma}$, respectively, and f is the frequency. Here the Fourier transform is defined as:

$$a(f) = \int_{-\infty}^{\infty} e^{-2\pi i f t} \sigma(t) dt \,. \tag{11}$$

In (10), the ratio between actual source amplitude a and estimated source amplitude $\bar{a}$ has become independent of the source characteristics.

In the following chapters, we will study frequency-domain beamforming, starting from some basic principles of signal processing.

3 Elements of signal processing

3.1 Sampled microphone data

When the microphone membranes are subject to pressure fluctuations $\chi_n(t)$, an alternating current (AC) is induced, of which the potential (in Volts) is recorded by the data-acquisition system. Modern systems are equipped with an analogue/digital (A/D) converter that samples the alternating voltage at a given sample interval Δt, where each sample is stored in a given number of bits (typically 16). To obtain unsteady (acoustic) pressures

$$\chi_{n,k} = \chi_n(k\Delta t) \tag{12}$$

at the microphone locations, the stored voltages are multiplied with factors obtained from calibrations.

3.2 Fourier transformation of microphone data

3.2.1 Discrete Fourier transform

Complex pressure amplitudes $p_n(f)$ of microphone signals can be obtained by evaluating a discrete Fourier transform (DFT) for a block of K samples:

$$p_n(f) = \frac{2}{K} \sum_{k=1}^{K} \chi_{n,k} e^{-2\pi i f k \Delta t} \,. \tag{13}$$

If the block size K is a power of 2, i.e., if an integer number q exists for which

$$K = 2^q , \tag{14}$$

then a so-called Fast Fourier Transform (FFT; Ref. 13) can be applied to evaluate (13) at once, for the entire relevant range of frequencies, which is (Ref. 16):

$$f_j = \frac{j}{K\Delta t},\ j = 1,...,K/2-1 . \tag{15}$$

3.2.2 Aliasing

It is noted that the frequency upper limit in (15): $f_{K/2} = 1/(2\Delta t)$ equals half the sample frequency:

$$f_{\text{sam}} = 1/\Delta t . \tag{16}$$

In the literature (e.g. Ref. 16), this frequency is called “Nyquist frequency” or “folding frequency”. Evaluation of (13) above that frequency does not add anything, because

$$p_n(f) = p_n(f_{\text{sam}} - f)^* , \tag{17}$$

where the asterisk denotes complex conjugation. Thus, frequencies higher than the Nyquist frequency are treated as lower frequencies. This is an undesired phenomenon called “aliasing”. To avoid aliasing, the acoustic signal should pass through a “low pass filter” that cuts off frequencies above the Nyquist frequency, before entering the A/D converter.

3.2.3 Cross-powers

Auto-powers $C_{nn}(f)$ and cross-powers $C_{mn}(f)$ are defined by

$$C_{mn}(f) = \frac{1}{2} p_m(f) p_n^*(f) . \tag{18}$$

3.2.4 Relation with cross-spectral density function

The cross-correlation function of the signals from microphones *n* and *m* is defined as (Ref. 16):

$$R_{mn}(t) = \lim_{T_0 \to \infty} \frac{1}{T_0} \int_0^{T_0} \chi_m(\tau) \chi_n(\tau + t) d\tau . \tag{19}$$

The cross-spectral density function is defined as the Fourier transform of the cross-correlation function:

$$\hat{G}_{mn}(f) = \int_{-\infty}^{\infty} R_{mn}(t) e^{-2\pi i f t} dt \,. \tag{20}$$

In real life, we can not evaluate this infinite integral. We have to start from the assumption that the signals $\chi_n(t)$ are periodic with some period *T*. Then, the same holds for the cross-correlation $R_{mn}(\tau)$ and equation (20) can be expressed as (Ref. 17):

$$\hat{G}_{mn}(f) = \sum_{j=-\infty}^{\infty} \frac{1}{T} \int_0^T R_{mn}(t) e^{-2\pi i f t} dt \times \delta\left(f - j/T\right), \tag{21}$$

where δ is the Dirac-delta function. The periodicity further implies that the limit variable T_0 in (19) can be replaced by *T*. It follows that (21) can be rewritten as:

$$\hat{G}_{mn}(f) = \sum_{j=-\infty}^{\infty} \hat{p}_m^*(f) \hat{p}_n(f) \delta\left(f - j/T\right), \tag{22}$$

where

$$\hat{p}_n(f) = \frac{1}{T} \int_0^T \chi_n(t) e^{-2\pi i f t} dt \,. \tag{23}$$

The cross-spectral density function, as defined in (22) is valid for positive as well as for negative frequency *f*. Usually, only positive frequencies are considered. For that purpose, the "single-sided" cross-spectral density function is defined as:

$$G_{mn}(f) = 2\hat{G}_{mn}(f), \, f > 0 \,. \tag{24}$$

We can derive:

$$G_{mn}(f) = \frac{1}{2} \sum_{j=1}^{\infty} p_m^*(f) p_n(f) \delta\left(f - j/T\right), \tag{25}$$

where

$$p_n(f) = 2\hat{p}_n(f) = \frac{2}{T}\int_0^T \chi_n(t) e^{-2\pi i f t} dt \,, \tag{26}$$

which is the continuous version of (13). Thus, we can write for the cross-spectral density:

$$G_{mn}(f) = \sum_{j=-\infty}^{\infty} C_{mn}^*(f)\delta\left(f - j/T\right). \tag{27}$$

Note that the cross-powers are defined in terms of the complex conjugate of the cross-spectral density function. This is for convenience in the further analysis.

3.2.5 Windows

For reduction of frequency side-lobes, a "window" u_k, $k = 1,..,K$ (Ref. 18) may be applied to (13):

$$p_n(f) = \frac{2}{K}\sum_{k=1}^{K} u_k \chi_{n,k} e^{-2\pi i f k \Delta t} \,. \tag{28}$$

An often used window is the so-called "Hanning window":

$$u_k = \sin^2\left(\pi k/K\right). \tag{29}$$

The features of this window and many more windows can be found in reference 18.

In order to obtain results comparable to a "rectangular window" ($u_k \equiv 1$), the numbers u_k have to be normalised somehow. Correct amplitudes (for tonal noise) are found when

$$\frac{1}{K}\sum_{k=1}^{K} u_k = 1 \,. \tag{30}$$

Correct auto- and cross-power levels (for broadband noise) are found when

$$\frac{1}{K}\sum_{k=1}^{K} u_k^2 = 1 \,. \tag{31}$$

3.2.6 Averaging

As derived in section 3.2.4, definition (18) for the cross-powers assumes a periodic signal, which is not true for broadband noise. However, if the signal is stationary (statistically expected properties are independent of starting sample), we can average the cross-powers over many blocks of K samples. Thus, statistical variations are averaged out.

To minimise numerical errors, the average values should be evaluated as a sequence:

$$\langle C \rangle_\nu = \big((\nu-1)\langle C \rangle_{\nu-1} + C_\nu\big)\big/\nu \,. \tag{32}$$

In the sequel, it will not explicitly be mentioned that cross-powers are the result of averaging.

4 Frequency-domain beamforming

4.1 Source model

Phased array beamforming is always done under the assumption of a certain source description. For example, in Section 2, (potential) monopole sources are assumed. The frequency-domain version of this monopole description is:

$$p(\vec{x},f) = \frac{a(f)e^{-2\pi i f \Delta t_e}}{4\pi \left\| \vec{x} - \vec{\xi} \right\|}, \tag{33}$$

where $\vec{\xi}$ is the monopole position, $a(f)$ the pressure amplitude (11), and Δt_e the emission time delay. We write (33), more generally, as a source model:

$$p(\vec{x},f) = a(f)g(\vec{x},f) \,. \tag{34}$$

Herein, g is called the "steering function". In (33), this steering function is in fact the "Green's function" of the Helmholtz equation, i.e., the solution of:

$$\nabla^2 g + \left(\frac{2\pi f}{c}\right)^2 g = -\delta(\vec{x} - \vec{\xi}) \,. \tag{35}$$

We may also include a uniform wind speed $\vec{U}$ in the source description, for instance when beamforming is done in a wind tunnel. Then the *convective* Helmholtz equation has to be considered, and the steering function is the solution of:

$$\nabla^2 g - \frac{1}{c^2}\left(2\pi i f + \vec{U}\cdot\nabla\right)^2 g = -\delta(\vec{x}-\vec{\xi})\,. \tag{36}$$

The solution of (36) reads:

$$g = \frac{e^{-2\pi i f \Delta t_e}}{4\pi\sqrt{\left(\vec{M}\cdot(\vec{x}-\vec{\xi})\right)^2 + \beta^2\left\|\vec{x}-\vec{\xi}\right\|^2}}, \tag{37}$$

in which $\vec{M}$ is a vector of Mach numbers:

$$\vec{M} = \vec{U}/c \tag{38}$$

and

$$\beta^2 = 1 - \left\|\vec{M}\right\|^2. \tag{39}$$

Instead of monopoles, the source model (34) can also be used for dipoles, quadrupoles, and all sorts of combinations (multipoles), simply by considering partial derivatives of (37). For acoustic arrays, this usually does not add much to the monopole description, because the array covers only a small portion of the solid angle of the directivity pattern of a source. Therefore, if the array is sufficiently far away, the source will be detected as if it were a monopole.

The source model (34) may even be used for plane waves (far-field beamforming). Then we have

$$g(\vec{x}, f) = \exp\left[i\vec{\alpha}\cdot\vec{x}\right], \tag{40}$$

in which the wave number vector $\vec{\alpha}$ must satisfy the dispersion relation:

$$\left(2\pi f/c + \vec{M}\cdot\vec{\alpha}\right)^2 - \left\|\vec{\alpha}\right\|^2 = 0\,. \tag{41}$$

In the case of far-field beamforming, the process of scanning is not done through a plane of potential source locations $\vec{\xi}$, but through a set of potential sound directions, defined by $\vec{\alpha}$.

4.2 Vector-matrix notation

From now on, we will write the array-related quantities as *N*-dimensional vectors and matrices. Furthermore, for brevity, we will omit the frequency dependence "(f)". This means that the pressure amplitudes, (13), are put in an *N*-dimensional vector **p**:

$$\mathbf{p} = \begin{pmatrix} p_1(f) \\ \vdots \\ p_N(f) \end{pmatrix}. \tag{42}$$

Furthermore, the cross-power matrix **C** is introduced by:

$$\mathbf{C} = \frac{1}{2}\mathbf{p}\mathbf{p}^*, \tag{43}$$

where the asterisk means "complex conjugate transpose". The source description is put in the "steering vector" **g**: the components g_n are the steering functions at the microphone locations:

$$g_n = g(\vec{x}_n, f). \tag{44}$$

4.3 Conventional Beamforming

Complex amplitudes $\overline{a}$ of sources in $\vec{\xi}$ can be estimated by comparing the measured pressure vector **p** with the steering vector **g**. An often used approach to determine $\overline{a}$ is through minimisation of:

$$J = \left\| \mathbf{p} - \overline{a}\mathbf{g} \right\|^2. \tag{45}$$

The solution of this minimisation problem is:

$$\overline{a} = \frac{\mathbf{g}^*\mathbf{p}}{\left\| \mathbf{g} \right\|^2}. \tag{46}$$

In the case of broadband noise, it does not make sense to apply averaging (Section 3.2.6) to expression (46), because its phase will be different for each block of samples. Then, it is more convenient to consider estimated source auto-powers:

$$\bar{A} = \frac{1}{2}|\bar{a}|^2 = \frac{1}{2}\bar{a}\,\bar{a}^* = \frac{1}{2}\frac{\mathbf{g}^*\mathbf{p}}{\|\mathbf{g}\|^2}\left(\frac{\mathbf{g}^*\mathbf{p}}{\|\mathbf{g}\|^2}\right)^* = \frac{1}{2}\frac{\mathbf{g}^*\mathbf{p}\mathbf{p}^*\mathbf{g}}{\|\mathbf{g}\|^4} = \frac{\mathbf{g}^*\mathbf{C}\mathbf{g}}{\|\mathbf{g}\|^4}. \qquad (47)$$

Expression (47) is known as “Conventional Beamforming”. It is the frequency-domain counterpart of “Least Squares Beamforming” (Section 2.3).

5 Array Performance

5.1 Example with random array

5.1.1 Beam pattern

In this section, simulations are carried out with a planar array of 50 microphones positioned randomly on a disk of 2 m radius, in the plane $z = 0$. The microphone positions are shown in Figure 4. A monopole source is simulated 6 m above the array, in $(0, 0, 6)$. The frequency of the emitted sound is 2000 Hz. Using the Conventional Beamforming technique, an acoustic scan was made on a surface of 4×4 m^2, 6 m above the array. The result of this scan, i.e. the “source plot” or the “acoustic image” is shown in Figure 5. Such a source plot of a single source is called “beam pattern”. The results are presented in dB; the dynamic range of the plot (i.e., the range of the colour bar) is 16 dB.

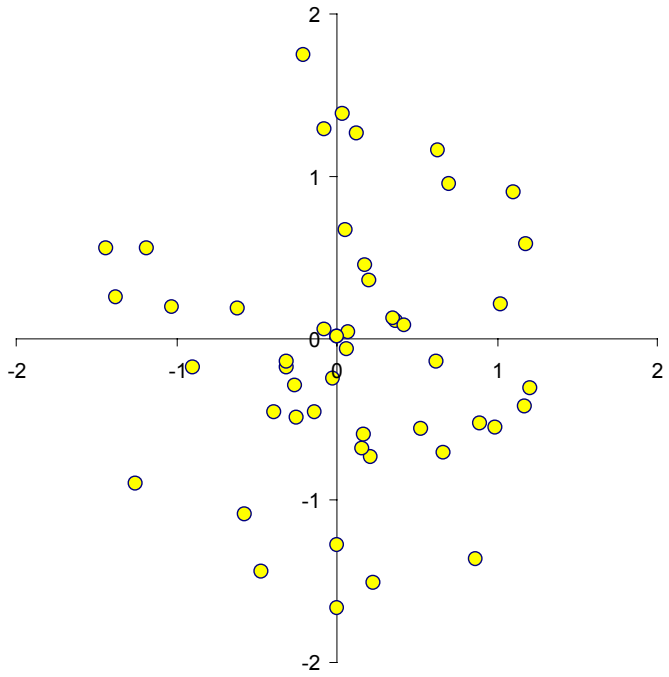

Figure 4 Random array of 50 microphones

5.1.2 Main lobe

In the centre of Figure 5, the source position can be recognised as the peak position. In the neighbourhood of the peak position, the estimated levels decrease with increasing distance from the source. Thus, a lobe appears: the so-called “main lobe” of the beam pattern. The width of the main lobe is a measure of the resolution of the array. Usually (Ref. 19), the resolution is defined as the width of the main lobe, 3 dB below its peak (see Figure 6).

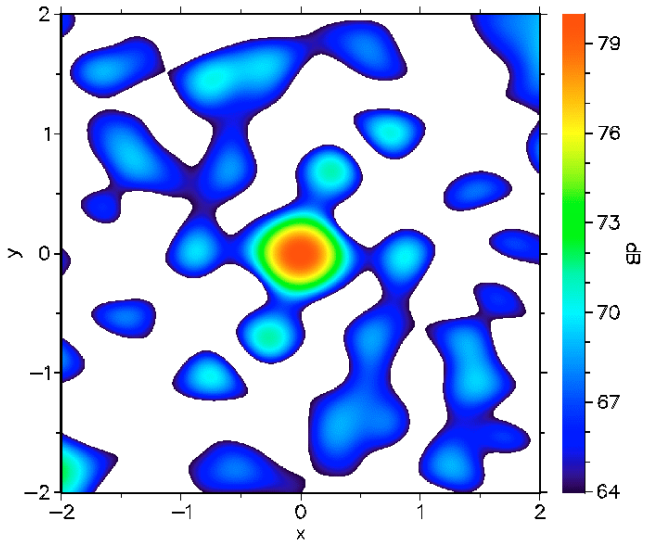

Figure 5 Source plot (z=6) with random array (z=0), f = 2000 Hz

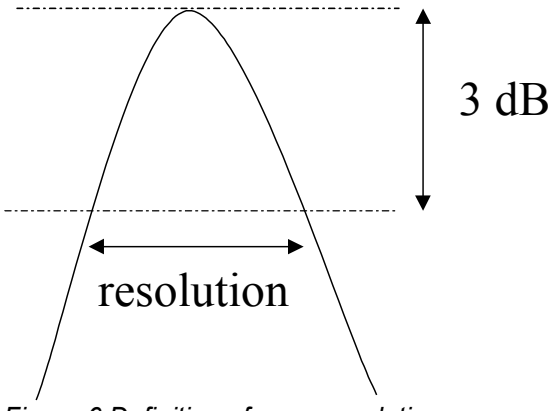

Figure 6 Definition of array resolution

The resolution of an array depends on its size, on frequency, on distance to the source, on the individual microphone positions, and on the used beamforming algorithm. Using Conventional Beamforming, a rule of thumb for the resolution of an array is:

$$\text{Resolution} = \frac{425Y}{Df}, \tag{48}$$

where Y is the distance between source and array, and D is the diameter of the array. In the example of Figure 5, the resolution is 38 cm, whereas the rule of thumb (48) yields 32 cm.

5.1.3 Side lobes

Apart from the main lobe, the beam pattern (Figure 5) also consists of "side lobes", i.e., local peaks. These side lobes are inevitable, due to the finite number of microphones. Since it is difficult to distinguish between the side lobes of a main source and the main lobe of a secondary source, it is desirable to keep the side lobe levels as low as possible. This is one of the main concerns in the design of a microphone layout (Refs. 20,21).

A measure for the array performance is its "dynamic range" or "array gain", which is defined as the difference between the peak level and the highest side lobe level of a beam pattern. This dynamic range depends on the number of microphones, microphone layout, source location, scanning grid, frequency and beamforming algorithm. The array gain of the example shown in Figure 5 is 8.5 dB.

5.2 Improvement of microphone layout

5.2.1 Aperture smoothing function

The issue of side lobes can be understood by considering far-field beamforming, i.e., by using the source model (40). Suppose that the incoming plane wave is described by

$$p(\vec{x}) = \exp\left[i\vec{\alpha}_0 \cdot \vec{x}\right]. \tag{49}$$

Then, the Conventional Beamforming algorithm (46) yields

$$a = \frac{1}{N}\sum_{n=1}^{N} \exp\left[i\left(\vec{\alpha}_0 - \vec{\alpha}\right)\cdot \vec{x}_n\right]. \tag{50}$$

Expression (50) can be written as

$$a = W\left(\vec{\alpha}_0 - \vec{\alpha}\right), \tag{51}$$

where W is the "aperture smoothing function" (see also Ref. 13):

$$W(\vec{\alpha}) = \frac{1}{N}\sum_{n=1}^{N} \exp\left[i\vec{\alpha}\cdot\vec{x}_n\right]. \tag{52}$$

The ideal array should have an aperture smoothing function satisfying:

$$\begin{cases} W(\vec{0}) = 1 \\ W(\vec{\alpha}) = 0, \text{ for } \vec{\alpha} \neq \vec{0} \end{cases} \tag{53}$$

However, with a finite number of microphones this is impossible. The local peak values of W for $\vec{\alpha} \neq \vec{0}$ represent side lobes.

5.2.2 Reduction of side lobes by array design

A possibility to reduce side lobe levels is to minimise, as a function of microphone positions, the following expression:

$$J\left(\vec{x}_1,...,\vec{x}_N\right) = \iiint\limits_{\alpha_{\min}\le\|\vec{\alpha}\|\le\alpha_{\max}} \left|W(\vec{\alpha})\right|^2 \mathrm{d}\,\vec{\alpha} = \frac{1}{N^2} \iiint\limits_{\alpha_{\min}\le\|\vec{\alpha}\|\le\alpha_{\max}} \left|\sum_{n=1}^{N} \exp\left[i\vec{\alpha}\cdot\vec{x}_n\right]\right|^2 \mathrm{d}\,\vec{\alpha}. \tag{54}$$

The bounds $\alpha_{\min}$ and $\alpha_{\max}$ depend on the array requirements. In practice, $\alpha_{\min}$ depends on the array diameter, and $\alpha_{\max}$ on the maximum frequency.

For a two-dimensional (planar) array, we can analogously minimise:

$$J\left(x_1,...,x_N,y_1,...,y_N\right) = \frac{1}{N^2} \iint\limits_{\alpha_{\min}^2\le\alpha_x^2+\alpha_y^2\le\alpha_{\max}^2} \left|\sum_{n=1}^{N} \exp\left[i\left(\alpha_x x_n + \alpha_y y_n\right)\right]\right|^2 \mathrm{d}\,\alpha_x\,\mathrm{d}\,\alpha_y. \tag{55}$$

Practical choices for $\alpha_{\min}$ and $\alpha_{\max}$ are:

$$\alpha_{\min} = \frac{3.83}{D}, \tag{56}$$

$$\alpha_{\max} = \pi\frac{f_{\max}}{c}, \tag{57}$$

where $f_{\max}$ is the maximum frequency to be analysed.

Expression (55) can be evaluated as:

$$
\begin{aligned}
&J\left(x_1,\ldots,x_N,y_1,\ldots,y_N\right)\\
&\quad=\frac{1}{N^2}\sum_{m=1}^{N}\sum_{n=1}^{N}\iint\limits_{\alpha_{\min}^2\le\alpha_x^2+\alpha_y^2\le\alpha_{\max}^2}\exp\left[i\left(\alpha_x(x_m-x_n)+\alpha_y(y_m-y_n)\right)\right]\mathrm{d}\alpha_x\,\mathrm{d}\alpha_y \qquad (58)\\
&\quad=\frac{1}{N^2}\sum_{m=1}^{N}\sum_{n=1}^{N}\int_{\alpha_{\min}}^{\alpha_{\max}} r\int_{0}^{2\pi}\exp\left[irR_{mn}\cos(\theta)\right]\mathrm{d}\theta\,\mathrm{d}r,
\end{aligned}
$$

in which

$$
R_{mn}^2=(x_m-x_n)^2+(y_m-y_n)^2\,. \qquad (59)
$$

Using some properties of Bessel functions (Ref. 22), we can evaluate (58) further as:

$$
\begin{aligned}
&J\left(x_1,\ldots,x_N,y_1,\ldots,y_N\right)=\frac{1}{N^2}\sum_{m=1}^{N}\sum_{n=1}^{N}\int_{\alpha_{\min}}^{\alpha_{\max}}2\pi rJ_0(rR_{mn})\,\mathrm{d}r\\
&\quad=\frac{\pi}{N^2}\left\{\sum_{n=1}^{N}\int_{\alpha_{\min}}^{\alpha_{\max}}2r\,\mathrm{d}r-2\sum_{m=1}^{N}\sum_{\substack{n=1\\m\neq n}}^{N}\frac{1}{R_{mn}}\int_{\alpha_{\min}}^{\alpha_{\max}}\frac{\mathrm{d}}{\mathrm{d}r}\left(rJ_0'(rR_{mn})\right)\mathrm{d}r\right\} \qquad (60)\\
&\quad=\frac{\pi}{N^2}\left\{N\left(\alpha_{\max}^2-\alpha_{\min}^2\right)-2\sum_{m=1}^{N}\sum_{\substack{n=1\\m\neq n}}^{N}\frac{\alpha_{\max}J_0'(\alpha_{\max}R_{mn})-\alpha_{\min}J_0'(\alpha_{\min}R_{mn})}{R_{mn}}\right\},
\end{aligned}
$$

in which J_0 is the zero-th order Bessel function of the first kind. Expression (60) can be minimised as a function of the parameters x_n and y_n. Since the derivatives of J can be evaluated analytically, this minimisation can be done relatively quickly by using, for example, the Conjugate Gradient Method (Ref. 23).

5.2.3 Example with optimised array

Using the optimisation procedure described in Section 5.2.2 and the random array of Figure 4 as starting positions, an optimised array was calculated. The result is shown in Figure 7. With this optimised array, the same simulation was carried out as in Section 5.1.1. The beam pattern of the simulated source is shown in Figure 8. Compared to the result with the random array (Figure 5), the resolution (width of main lobe) is virtually the same. However the side lobe levels are clearly lower. Instead of 8.5 dB in Figure 5, the array gain is now 12.5 dB.

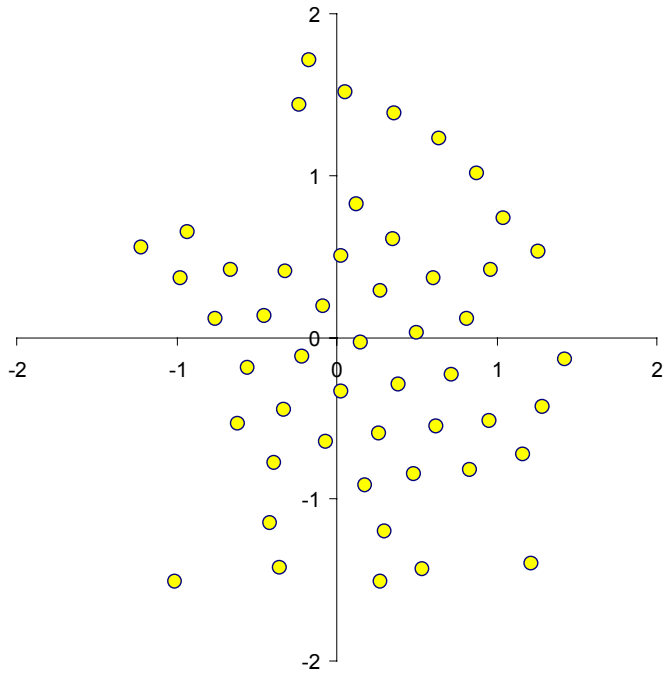

Figure 7 Optimised array

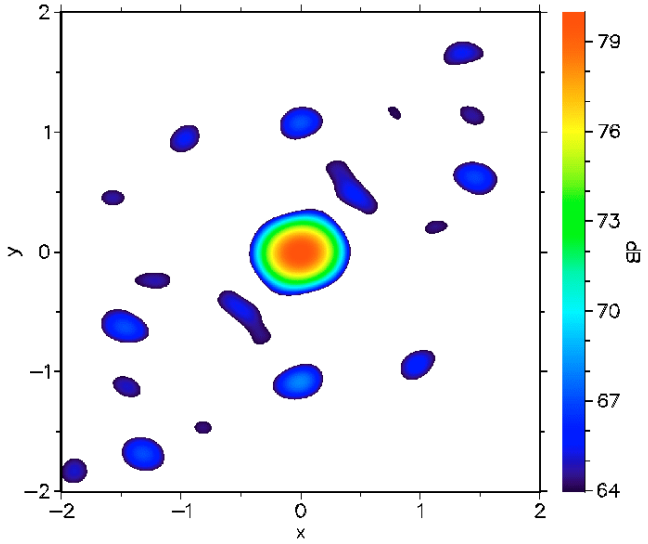

Figure 8 Source plot with optimised array, f = 2000 Hz

6 Advanced methods

6.1 Beamforming without auto-powers

In wind tunnel measurements, microphone auto-powers have much higher levels than the corresponding cross-powers. In other words, the main diagonal components of the cross-power

matrix **C** have much higher levels than the off-diagonal components. There can be two reasons for this phenomenon, which are discussed below.

6.1.1 Wind noise (boundary layer noise)

When a microphone is placed in the wind, it will detect not only acoustic pressures, but also pressure disturbances of hydrodynamic nature due to the turbulent boundary layer around the microphone. This typically occurs in closed wind tunnel test sections, where the microphones are mounted flush in a wall. Because wind noise is incoherent from one microphone to the other (except when microphones are placed very close to each other in the wind direction, and then only for very low wave numbers), it will appear only in the auto-powers, and not in the cross-powers.

In mathematics: suppose that the pressure vector **p** is composed of an acoustic component $\mathbf{p}_a$ and a wind noise component $\mathbf{p}_w$. Then for the cross-power matrix we have

$$\mathbf{C} = \frac{1}{2}\left(\mathbf{p}_a + \mathbf{p}_w\right)\left(\mathbf{p}_a^* + \mathbf{p}_w^*\right) = \frac{1}{2}\mathbf{p}_a\mathbf{p}_a^* + \frac{1}{2}\mathbf{p}_a\mathbf{p}_w^* + \frac{1}{2}\mathbf{p}_w\mathbf{p}_a^* + \frac{1}{2}\mathbf{p}_w\mathbf{p}_w^*. \tag{61}$$

The second and the third term in the right hand side disappear through averaging, and what remains is:

$$\mathbf{C} = \frac{1}{2}\mathbf{p}_a\mathbf{p}_a^* + \frac{1}{2}\mathbf{p}_w\mathbf{p}_w^* = \mathbf{C}_a + \mathbf{C}_w \tag{62}$$

The wind noise induced matrix $\mathbf{C}_w$ has, in the limit, only non-zero components on the main diagonal.

6.1.2 Loss of coherence

When sound travels through a turbulent medium, it deforms (Refs. 24-27). When sound from a noise source travels along different paths through a turbulent medium, it will deform differently. As a result, the phase of the cross-power between two microphones will be distorted compared to the non-deformed case. Therefore, after averaging, the cross-power levels are lower than in the non-deformed case. This reduction of cross-power level is dependent on the level of the turbulence, the distance between the microphones, the distance between source and microphone and on frequency. Since auto-powers do not contain phase information, their levels are not affected by coherence loss. Hence, auto-powers tend to dominate the cross-power matrix when coherence loss becomes significant.

Loss of coherence is in particular an important issue for measurements in an open test section of a wind tunnel (Ref. 24), when the array is placed out of the flow and the sound has to travel through the turbulent shear layer. Typically, it makes source location impossible for frequencies higher than 20 kHz. Loss of coherence is also an issue for outdoor measurements (Refs. 25-27), for instance for fly-over measurements (Ref. 28). For those measurements, the turbulence in the atmospheric boundary layer is the cause.

6.1.3 Elimination of auto-powers

In the cases where the auto-powers prevail against the cross-powers, much "cleaner" noise maps are obtained when the auto-powers are not used in the beamforming process. For that purpose, we can generalise the Conventional Beamforming method of Section 4.3 as follows.

Instead of (45), we can equivalently minimise:

$$J = \left\| \mathbf{C} - \overline{A}\mathbf{g}\mathbf{g}^* \right\|^2 = \sum_{m=1}^{N}\sum_{n=1}^{N} \left| C_{mn} - \overline{A} g_m g_n^* \right|^2 . \tag{63}$$

This can be generalised into

$$J = \sum_{(m,n)\in S}^{N} \left| C_{mn} - \overline{A} g_m g_n^* \right|^2 , \tag{64}$$

where S is a sub-set of all possible (m,n)-combinations. For instance in case of auto-power elimination:

$$S = \left\{ (m,n) \in [1...N] \times [1...N]; m \neq n \right\} . \tag{65}$$

The solution of minimising (64) is:

$$\overline{A} = \sum_{(m,n)\in S}^{N} g_m^* C_{mn} g_n \Bigg/ \sum_{(m,n)\in S}^{N} \left| g_m \right|^2 \left| g_n \right|^2 . \tag{66}$$

The strength of this method is illustrated by array measurements in the DNW-LST on a half model of the Fokker 100 aircraft (Figure 9). These measurements were used to test flap tip devices (Ref. 31). An array of 96 microphones was used, mounted flush in the wall (red surface in Figure 9). In Figure 10, typical results are shown of beamforming with and without auto-

powers. The necessity of beamforming without auto-powers in this situation is clearly demonstrated.

A caution to this method is that the estimated source auto-power $\overline{A}$, as calculated by (66) may have a negative value, because the governing matrix is not positive-definite anymore. Since negative auto-powers are not physical, those results should be rejected.

Figure 9 Array measurements on a Fokker 100 half model in DNW-LST

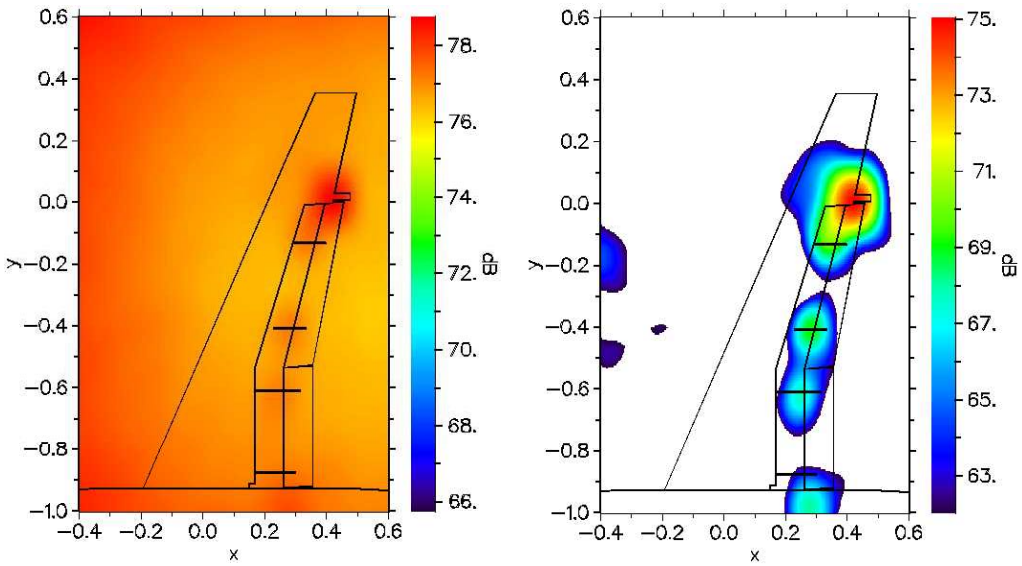

Figure 10 Source plots of Fokker 100 half model; comparison between beamforming with (left) and without (right) auto-powers

6.2 The use of eigenvalue analysis

When auto-powers are not dominating (for instance, for array measurements in an anechoic chamber), an eigenvalue analysis of the cross-power matrix can be useful. Herewith, the

measured acoustic pressure can be split into incoherent “principal” components. This analysis can be used for

a) determining the number of incoherent sources,
b) increasing the processing speed,
c) noise filtering.

The analysis is as follows:

Suppose there are L independent sources:

$$\mathbf{p} = \sum_{l=1}^{L} \mathbf{p}_l \,. \tag{67}$$

For the cross-power matrix, we have

$$\mathbf{C} = \frac{1}{2}\left(\sum_{l=1}^{L} \mathbf{p}_l \right)\left(\sum_{l=1}^{L} \mathbf{p}_l \right)^{*} = \frac{1}{2}\sum_{l_1=1}^{L}\sum_{l_2=1}^{L} \mathbf{p}_{l_1}\mathbf{p}_{l_2}^{*} \,. \tag{68}$$

After averaging, the following expression remains:

$$\mathbf{C} = \frac{1}{2}\sum_{l=1}^{L} \mathbf{p}_l\mathbf{p}_l^{*} \,. \tag{69}$$

Herewith, $\mathbf{C}$ is a matrix with rank L. In other words, the number of non-zero eigenvalues of $\mathbf{C}$ is equal to the number of incoherent sources. Since the matrix $\mathbf{C}$ is Hermitian (invariant to complex conjugate transposition) and positive definite, its eigenvalues e_λ are non-negative and the corresponding eigenvectors form an orthogonal set. The eigenvectors of $\mathbf{C}$ or "principal components" correspond to virtual sources, which need not coincide with the physical incoherent sources.

The cross-power matrix $\mathbf{C}$ can be written as

$$\mathbf{C} = \mathbf{Q}\mathbf{E}\mathbf{Q}^{*}, \tag{70}$$

where $\mathbf{E}$ is an $L \times L$ diagonal matrix containing the non-zero eigenvalues and $\mathbf{Q}$ is an $N \times L$ matrix, the columns of which are the normalised eigenvectors of $\mathbf{C}$. For the Conventional Beamforming algorithm (47) we then have

$$\bar{A} = \frac{\mathbf{g}^* \mathbf{Q} \mathbf{E} \mathbf{Q}^* \mathbf{g}}{\|\mathbf{g}\|^4} . \tag{71}$$

In general, the matrix $\mathbf{C}$ will not have a number (L) of non-zero and a number ($N - L$) of zero eigenvalues. The reality will be that $\mathbf{C}$ has a full spectrum. If the signal-to-noise ratio is sufficiently high, then the signals can be recognised in the space spanned by the eigenvectors corresponding to the highest eigenvalues. In other words, if a number of eigenvalues has significantly higher values than the rest, they can be attributed to incoherent sources. The lower eigenvalues represent noise, which can be filtered out by replacing the lowest eigenvalues by zero.

When one principal component is dominant, we can enlarge the array gain by filtering this component out, viz. removing from the cross-power matrix the eigenvector corresponding to the highest eigenvalue (Ref. 29). A successful application of this technique is described in reference 30.

6.3 Adaptive beamforming

Again, when relatively high auto-power levels is not an important issue, special techniques can be applied to enhance the resolution. One of these high-resolution techniques is "Robust Adaptive Beamforming" (Ref. 32). This technique is discussed below. For a better understanding, we will also reformulate the definition of Conventional Beamforming and discuss the "Minimum Variance Method" (Ref. 13).

6.3.1 Reformulation of Conventional Beamforming

Using a full cross-power matrix, a general beamforming expression is:

$$\bar{A} = \mathbf{w}^* \mathbf{C} \mathbf{w} , \tag{72}$$

where $\mathbf{w}$ is a weight vector that is dependent on the steering vector **g**. The weight vector has to be such that unit gain is found for unit sources in the look direction:

$$\mathbf{w}^* \mathbf{g} = 1 . \tag{73}$$

Obviously, there are many possible choices for **w** that fulfil (73). One of them is obtained by minimising the squared norm of the weight vector:

$$J = \|\mathbf{w}\|^2 . \tag{74}$$

The solution of the minimisation problem (74) with constraint (73) is

$$\mathbf{w} = \frac{\mathbf{g}}{\mathbf{g}^* \mathbf{g}} . \tag{75}$$

Substitution of (75) into (72) yields the same expression as (47). In other words, we have found an alternative definition of Conventional Beamforming.

Since its weight vector is the one with the smallest possible norm, Conventional Beamforming is the most robust beamforming technique available. That is, inaccuracies in source characteristics (i.e., steering vector **g**), in source position or in microphone calibrations lead to the smallest possible errors in the array output (72). Moreover, there is not much sensitivity to noise. Therefore, the Conventional Beamforming technique (though without auto-powers) is very suitable for wind tunnel measurements.

6.3.2 Minimum Variance Method

Another beamforming method is obtained by minimising the array output (72), again under the constraint (73). The optimum weight vector **w** is:

$$\mathbf{w} = \frac{\mathbf{C}^{-1}\mathbf{g}}{\mathbf{g}^* \mathbf{C}^{-1}\mathbf{g}} . \tag{76}$$

Hence, for the source strength $\overline{A}$, (72), we find

$$\overline{A} = \frac{1}{\mathbf{g}^* \mathbf{C}^{-1}\mathbf{g}} . \tag{77}$$

This method is known as the "Minimum Variance Method" (Ref. 13). It is a so-called “adaptive” method, because the weight vector **w** depends on the measured results. Theoretically, the Minimum Variance Method yields very low side lobe levels and very high resolution. However, the method is unstable ("non-robust") if $\mathbf{C}$ is ill-conditioned, which is the case when the signal-to-noise ratio is high (sic). Then, predicted results are very sensitive to small mismatches.

6.3.3 Robust Adaptive Beamforming

To overcome the drawbacks of the Minimum Variance Method, Cox et al. (Ref. 32) proposed a method called "Robust Adaptive Beamforming", in which some artificial “wind noise” is added to $\mathbf{C}$. Then, the expression

$$J = \mathbf{w}^* \left(\mathbf{C} + \mu \mathbf{I} \right) \mathbf{w} , \tag{78}$$

has to be minimised, under the same constraint (73). In (78), **I** is the identity matrix and μ is a control parameter. By rewriting (78) as:

$$J = \mathbf{w}^* \mathbf{C} \mathbf{w} + \mu \left\| \mathbf{w} \right\|^2 , \tag{79}$$

it becomes clear that actually a controlled combination of array output and weight vector norm is minimised. The solution of the minimisation problem is:

$$\mathbf{w} = \frac{\left(\mathbf{C} + \mu \mathbf{I} \right)^{-1} \mathbf{g}}{\mathbf{g}^* \left(\mathbf{C} + \mu \mathbf{I} \right)^{-1} \mathbf{g}} . \tag{80}$$

For the source auto-power $\overline{A}$, (72), we have

$$\overline{A} = \frac{\mathbf{g}^* \left(\mathbf{C} + \mu \mathbf{I} \right)^{-1} \mathbf{C} \left(\mathbf{C} + \mu \mathbf{I} \right)^{-1} \mathbf{g}}{\left(\mathbf{g}^* \left(\mathbf{C} + \mu \mathbf{I} \right)^{-1} \mathbf{g} \right)^2} . \tag{81}$$

To control the robustness of the method, we put a constraint on the norm of the weight vector. It is demanded that the ratio $\left\| \mathbf{w} \right\| / \left\| \mathbf{w}_{CB} \right\|$, where $\mathbf{w}_{CB}$ is the weight vector (75) of Conventional Beamforming, should not exceed a prescribed value. In the literature (Ref. 33), this is called the "White Noise Gain Constraint" WNC, which is expressed in dB:

$$10^{10} \log \left[\left(\mathbf{w}^* \mathbf{w} \right) / \left(\mathbf{w}_{CB}^* \mathbf{w}_{CB} \right) \right] = 10^{10} \log \left[\left(\mathbf{w}^* \mathbf{w} \right) \left(\mathbf{g}^* \mathbf{g} \right) \right] \le \mathrm{WNC} . \tag{82}$$

By definition, we have $\mathrm{WNC} = 0$ for Conventional Beamforming and $\mathrm{WNC} > 0$ otherwise. Typically, a few dB is used as value for WNC.

In Figure 11 a source plot is shown, obtained with Robust Adaptive Beamforming with $\mathrm{WNC} = 1$ dB. It is for the same (optimised) array as in Section 5.2.3, and for the same source simulation. Compared with Figure 8, the main lobe has become narrower (higher resolution) and the side lobes are disappeared (higher array gain).

Indeed, Robust Adaptive Beamforming is a very powerful tool in "clean" situations (anyhow in simulation, but also, for instance, in anechoic chambers). However, in the case of high auto-

powers, the method is no longer applicable. Also, in cases with much uncertainty (about array positions, microphone sensitivities, source model), the lack of robustness may spoil the results.

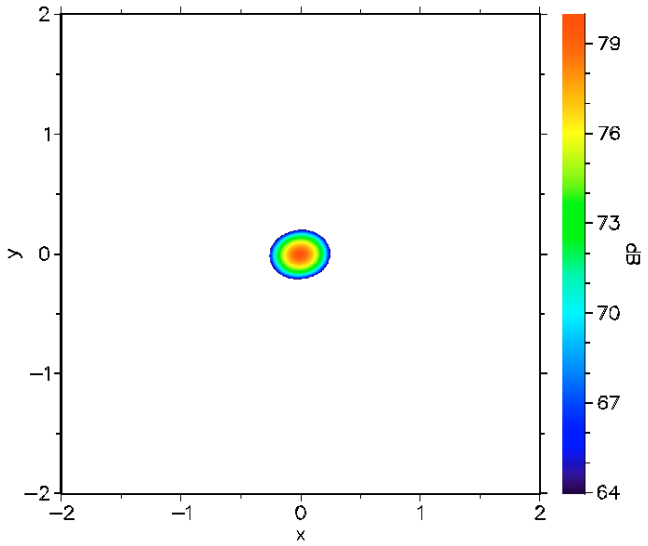

Figure 11 Source plot with optimised array, f = 2000 Hz, Robust Adaptive Beamforming, WNC = 1 dB

6.4 Source power integration

Using Conventional Beamforming, absolute source powers can be extracted from array measurements only under the following restrictions:

- The sources are point sources.
- The source directivity is uniform, at least in the direction of the array.
- The resolution of the beamforming method is high enough to separate different sources.
- There is no loss of coherence.

If the requirements above are fulfilled then the source powers can be found as the (local) peak values in the acoustic source plots.

However, in wind tunnel measurements these requirements are seldom fulfilled. To obtain absolute levels nonetheless, a source power integration technique was developed (Ref. 33). Basically, the integration technique sums the source auto-power estimates for all points of a scanning grid. Afterwards, the result is scaled such that the exact result is obtained for a simulated point source in the centre of the grid.

For successful application of the integration technique, Conventional Beamforming should be used for the source auto-power estimates. Conventional Beamforming including auto-powers (Section 4.3) is preferred. Conventional Beamforming without auto-powers (Section 6.1.3) is possible too, however with some caution. Both methods are discussed below.

The source power integration technique can be applied also to sub-sets of the scanning grid. Thus, the source power contributions from several parts of a research model can easily be compared.

6.4.1 Standard method

Suppose H is the number of points in a scanning grid, and $\overline{A}_{s,h},\ h=1,...,H,$ are the beamforming results (source auto-power estimates) of a simulated point source, somewhere in the middle of the grid, which has source auto-power P_s. Suppose further that $\overline{A}_h,\ h=1,...,H,$ are the beamforming results from measurements. Then, the integrated source power estimate is:

$$P=\frac{\sum_{h=1}^{H}\overline{A}_h}{\sum_{h=1}^{H}\overline{A}_{s,h}}\times P_s\,. \tag{83}$$

For several wind tunnel array measurements, reference 33 reported good agreement with levels of individual microphones. This reference also discusses more advanced methods, using several reference sources instead of one. Usually, application of these advanced methods is not necessary.

6.4.2 Method without auto-powers

Because of the relatively high auto-power levels in wind tunnel measurements, it is convenient to have available also an integration procedure without auto-powers. In closed test sections, the microphone auto-powers are often dominated by boundary layer noise, and the standard integration technique does not give the correct answers. In open test sections (using an out-of-flow microphone array), elimination of auto-powers is convenient to see more details when more than one integration (sub-) grid is considered.

However, straightforward application of (83) may lead to poor results. The source auto-power estimates $\overline{A}_h$ and $\overline{A}_{s,h}$ can be both positive and negative, which makes expression (83) unstable. A good alternative is to consider only the positive source auto-power estimates:

$$P=\frac{\sum_{h=1}^{H}\max\left(\overline{A}_h,0\right)}{\sum_{h=1}^{H}\max\left(\overline{A}_{s,h},0\right)}\times P_s\,. \tag{84}$$

The following, more refined method considers only the source auto-power estimates that are less than Z dB (typically 10 dB) below the peak levels $\overline{A}_{\max}$ and $\overline{A}_{s,\max}$. In other words, power estimates that are more than Z dB below the peak values are neglected. Thus, we have for the integrated source power:

$$P = \frac{\sum_{h=1}^{H} \tilde{A}_h}{\sum_{h=1}^{H} \tilde{A}_{s,h}} \times P_s , \tag{85}$$

where

$$\tilde{A}_h = \begin{cases} 0, \text{ if } \overline{A}_h \le 0 \text{ or } 10^{10} \log\left(\overline{A}_h / \overline{A}_{\max}\right) \le -Z, \\ \overline{A}_h, \text{ otherwise,} \end{cases} \tag{86}$$

and

$$\tilde{A}_{s,h} = \begin{cases} 0, \text{ if } \overline{A}_{s,h} \le 0 \text{ or } 10^{10} \log\left(\overline{A}_{s,h} / \overline{A}_{s,\max}\right) \le -Z, \\ \overline{A}_{s,h}, \text{ otherwise.} \end{cases} \tag{87}$$

The integration method without auto-power loses its ability to predict correct levels, when coherence loss becomes significant. This is especially the case in open wind tunnel test sections. This technique is, nevertheless, still convenient as a tool to compare different integration areas and different model configurations.

7 Moving sources

For array measurements on moving objects, the correct acoustic transfer function from moving source to receiver is required (source model), incorporating the effect of Doppler frequency shift (Refs. 10, 11). For that purpose, an expression has to be used for a moving monopole source in a uniform flow. A brief derivation of such an expression is given below. For a more thorough approach, the reader is referred to reference 34. Using this transfer function, and by proper interpolation of the sampled microphone data, the emitted signals can be estimated. This is necessarily a time-domain technique. It will be explained, however, that the signal/noise ratio

can be enlarged by a technique, which is similar to the frequency-domain technique of removing the auto-powers (Section 6.1).

7.1 Source description

The acoustic pressure field χ of a monopole source moving in a uniform flow is governed by the differential equation:

$$\nabla^2\chi-\frac{1}{c^2}\left(\frac{\partial}{\partial t}+\vec{U}\cdot\nabla\right)^2\chi=-\sigma(t)\delta\left(\vec{x}-\vec{\xi}(t)\right), \tag{88}$$

in which $\vec{\xi}(t)$ is the time-dependent source position. Following reference 35, equation (88) can be solved by writing the right-hand side as a superposition:

$$\nabla^2\chi-\frac{1}{c^2}\left(\frac{\partial}{\partial t}+\vec{U}\cdot\nabla\right)^2\chi=-\int_{-\infty}^{\infty}\sigma(\tau)\delta\left(\vec{x}-\vec{\xi}(\tau)\right)\delta(t-\tau)d\tau\,. \tag{89}$$

Then, the solution can be expressed as

$$\chi(\vec{x},t)=\int_{-\infty}^{\infty}\sigma(\tau)G\left(\vec{x},\vec{\xi}(\tau),t,\tau\right)d\tau\,, \tag{90}$$

where G (the Green's function) is a solution of

$$\nabla^2G-\frac{1}{c^2}\left(\frac{\partial}{\partial t}+\vec{U}\cdot\nabla\right)^2G=-\delta\left(\vec{x}-\vec{\xi}(\tau)\right)\delta(t-\tau)\,. \tag{91}$$

The solution of (91) can be derived from the Green's function of the ordinary wave equation (Ref. 36) by using the following co-ordinate transformation:

$$\begin{cases}t_1=t,\\ \vec{x}_1=\vec{x}-\vec{U}t.\end{cases} \tag{92}$$

In the transformed system, we have:

$$\nabla_1^{\,2}G-\frac{1}{c^2}\frac{\partial^2G}{\partial t_1^{\,2}}=-\delta\left(\vec{x}_1+\vec{U}t_1-\vec{\xi}(\tau)\right)\delta(t_1-\tau)=-\delta\left(\vec{x}_1+\vec{U}\tau-\vec{\xi}(\tau)\right)\delta(t_1-\tau)\,. \tag{93}$$

The causal solution of (93) is:

$$G = \frac{\delta\left(t_1 - \tau - \frac{1}{c}\left\| \vec{x}_1 + \vec{U}\tau - \vec{\xi}(\tau) \right\| \right)}{4\pi \left\| \vec{x}_1 + \vec{U}\tau - \vec{\xi}(\tau) \right\|}. \tag{94}$$

Therefore, the causal solution of equation (91), in other words the pressure field induced by an impulsive blow in a uniform flow, is

$$G\left(\vec{x}, \vec{\xi}(\tau), t, \tau\right) = \frac{\delta\left(t - \tau - \frac{1}{c}\left\| \vec{x} - \vec{\xi}(\tau) - \vec{U}(t-\tau) \right\| \right)}{4\pi \left\| \vec{x} - \vec{\xi}(\tau) - \vec{U}(t-\tau) \right\|}, \tag{95}$$

in which $t > \tau$. It follows that the solution of (89) and hence the solution of (88) is

$$\chi(\vec{x}, t) = \int_{-\infty}^{\infty} \frac{\sigma(\tau)\delta\left(t - \tau - \frac{1}{c}\left\| \vec{x} - \vec{\xi}(\tau) - \vec{U}(t-\tau) \right\| \right)}{4\pi \left\| \vec{x} - \vec{\xi}(\tau) - \vec{U}(t-\tau) \right\|} d\tau. \tag{96}$$

To elaborate this integral, we introduce the emission time $\tau_e(t)$ as the solution of

$$t - \tau_e = \frac{1}{c}\left\| \vec{x} - \vec{\xi}(\tau_e) - \vec{U}(t - \tau_e) \right\|. \tag{97}$$

As long as the motion is subsonic, this solution is unique. Using (97) and the identity (Ref. 35)

$$\int_{-\infty}^{\infty} f(\tau)\delta\left(\gamma(\tau)\right) d\tau = \sum \frac{f(\tau_0)}{\left|\gamma'(\tau_0)\right|}, \text{ where } \gamma(\tau_0) = 0, \tag{98}$$

equation (96) can be worked out as

$$\chi(\vec{x}, t) = \frac{\sigma(\tau_e)}{4\pi\left\{ c\left(t - \tau_e\right) + \frac{1}{c}\left(-\vec{\xi}'(\tau_e) + \vec{U} \right) \cdot \left(\vec{x} - \vec{\xi}(\tau_e) - \vec{U}(t - \tau_e) \right) \right\}}. \tag{99}$$

It follows that the transfer function *F* from moving source in $\vec{\xi}(t)$ to receiver in $\vec{x}$ is given by

$$F\left(\vec{x},\vec{\xi}(\tau_e),t,\tau_e\right)=\frac{\chi(\vec{x},t)}{\sigma(\tau_e)}=\frac{1}{4\pi\left\{c\left(t-\tau_e\right)+\frac{1}{c}\left(-\vec{\xi}'(\tau_e)+\vec{U}\right)\cdot\left(\vec{x}-\vec{\xi}(\tau_e)-\vec{U}(t-\tau_e)\right)\right\}}, \tag{100}$$

where the relation between t and τ_e is given by equation (97).

7.2 Reconstruction of source signals

If a monopole source with time-dependent position $\vec{\xi}(t)$ is present, then we can write for the microphone signals

$$\chi_n(t)=F\left(\vec{x}_n,\vec{\xi}(\tau_e),t,\tau_e\right)\sigma(\tau_e)+\varepsilon_n(t), \tag{101}$$

where $\varepsilon_n(t)$ is noise and/or contributions from other sources.

In order to estimate the source signal $\bar{\sigma}(\tau)$ from the microphone signals $\chi_n(t)$, we take in equation (101) a fixed emission time τ_e, independent of microphone number. Then the receiver time t depends on n and it is better to write equation (101) as

$$\chi_n(t_n)=F\left(\vec{x}_n,\vec{\xi}(\tau_e),t_n,\tau_e\right)\sigma(\tau_e)+\varepsilon_n(t_n), \tag{102}$$

or, briefly,

$$\chi_n(t_n)=F_n(t_n,\tau_e)\sigma(\tau_e)+\varepsilon_n(t_n). \tag{103}$$

The microphone-dependent receiver times t_n follow from equation (97):

$$t_n-\tau_e=\frac{1}{c}\left\|\vec{x}_n-\vec{\xi}(\tau_e)-\vec{U}(t_n-\tau_e)\right\|. \tag{104}$$

Though in general an explicit solution τ_e as a function of t_n does not exist, we do have an explicit expression t_n as function of τ_e:

$$t_n=\tau_e+\Delta t_e, \tag{105}$$

with

$$\Delta t_e = \frac{1}{c\beta^2}\left(-\vec{M}\cdot\left(\vec{x}_n - \vec{\xi}(\tau_e)\right) + \sqrt{\left\{\vec{M}\cdot\left(\vec{x}_n - \vec{\xi}(\tau_e)\right)\right\}^2 + \beta^2 \left\|\vec{x}_n - \vec{\xi}(\tau_e)\right\|^2} \right). \tag{106}$$

An estimated source signal $\bar{\sigma}(\tau_e)$ can be found with the delay-and-sum procedure:

$$\bar{\sigma}(\tau_e) = \frac{1}{N}\sum_{n=1}^{N} \bar{\sigma}_n(\tau_e), \tag{107}$$

with

$$\bar{\sigma}_n(\tau_e) = \chi_n(t_n) / F_n(t_n, \tau_e). \tag{108}$$

It is noted that t_n, as calculated by (105), does not coincide with a sample time $k\Delta t$. The best way to proceed is to linearly interpolate the sampled data:

$$\chi_n(t_n) \approx \chi_{n,k}\left((k+1) - \frac{t_n}{\Delta t} \right) + \chi_{n,k+1}\left(\frac{t_n}{\Delta t} - k \right). \tag{109}$$

To avoid the frequency spectrum from being spoiled by side lobes from higher frequencies, the sample frequency should be taken higher than two times the maximum analysis frequency, without raising the low pass filter cut-off frequency. This problem was addressed for instance by Howell et al (Ref. 11).

7.3 Reconstruction of source auto-powers

7.3.1 Straightforward method

A straightforward way to calculate the frequency spectrum of a source signal is to evaluate equation (107) for $\tau_e = k\Delta t,\ k = 1, ..., K$ and then perform an FFT, resulting in pressure amplitudes:

$$\bar{a}(\bar{\sigma}) = \frac{1}{N}\sum_{n=1}^{N} \bar{a}(\bar{\sigma}_n). \tag{110}$$

The source auto-power estimate $\bar{A}$ is calculated as:

$$\overline{A} = \frac{1}{2}\left|\overline{a}(\overline{\sigma})\right|^2 = \frac{1}{2N^2}\left|\sum_{n=1}^{N}\overline{a}(\overline{\sigma}_n)\right|^2 = \frac{1}{2N^2}\sum_{m=1}^{N}\sum_{n=1}^{N}\overline{a}(\overline{\sigma}_m)\overline{a}(\overline{\sigma}_n)^* . \tag{111}$$

7.3.2 Error estimate

With equations (103), (108) and (111), we can write

$$\overline{A} = \frac{1}{2}\left|a(\sigma) + \frac{1}{N}\sum_{n=1}^{N}\overline{a}\left(\varepsilon_n / F_n\right)\right|^2 . \tag{112}$$

Now assume that $\varepsilon_n(t)$ is stochastic and incoherent from one microphone to the other (e.g. wind noise). Then, after averaging, the following expression remains:

$$\overline{A} = \frac{1}{2}\left|a(\sigma)\right|^2 + \frac{1}{2N^2}\sum_{n=1}^{N}\left|\overline{a}\left(\varepsilon_n / F_n\right)\right|^2 = A + \frac{1}{2N^2}\sum_{n=1}^{N}\left|\overline{a}\left(\varepsilon_n / F_n\right)\right|^2 , \tag{113}$$

where A is the true source power.

7.3.3 Alternative method

Consider the following approximation of equation (111):

$$\overline{A} = \frac{1}{2N(N-1)}\sum_{m=1}^{N}\sum_{\substack{n=1 \\ n\neq m}}^{N}\overline{a}(\overline{\sigma}_m)\overline{a}(\overline{\sigma}_n)^* = \frac{1}{2N(N-1)}\left(\left|\sum_{n=1}^{N}\overline{a}(\overline{\sigma}_n)\right|^2 - \sum_{n=1}^{N}\left|\overline{a}(\overline{\sigma}_n)\right|^2\right). \tag{114}$$

Again under the assumption that $\varepsilon_n(t)$ is stochastic and incoherent, and after averaging over many time periods, we simply get $\overline{A} = A$. In other words, the expected error is now zero.

This alternative method is analogous to the elimination of the main diagonal from the cross-power matrix (Section 6.1.3). Just like its frequency-domain counterpart, the right-hand side of equation (114) may become negative, which is not physical. This may happen, for instance, if a secondary source exists, giving a coherent contribution to $\varepsilon_n(t)$, or in case of insufficient averaging.

7.4 Applications

As examples of applications of the beamforming technique with moving sources, results are given of array measurements on a wind turbine model in the DNW-LLF (Refs. 12, 37), and on landing aircraft at Schiphol airport (Ref. 28). Typical source plots are shown in Figure 12 and Figure 13, respectively.

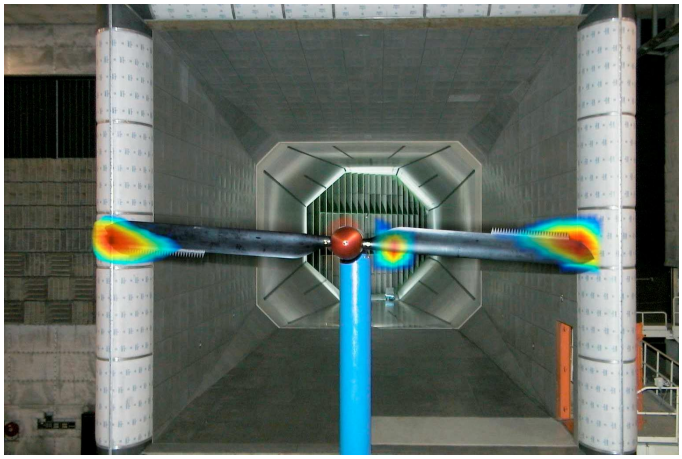

Figure 12 Wind turbine rotor in DNW-LLF

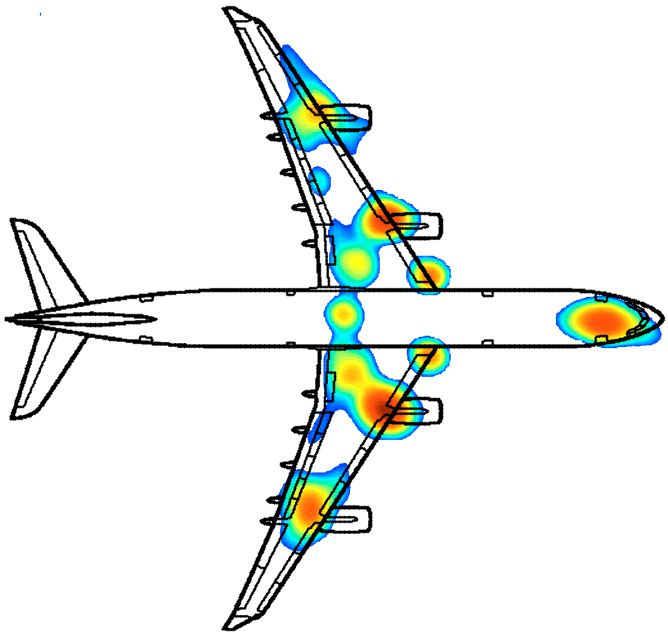

Figure 13 Airbus A340 during approach

8 References

1. Grosche, F.-R., Stiewitt, H., and Binder, B., "Acoustic wind-tunnel measurements with a highly directional microphone ", *AIAA Journal* Vol. 15., No. 11, pp. 1590-1596, 1977.
2. Schlinker, R.H., "Airfoil trailing edge noise measurements with a directional microphone", AIAA Paper 77-1269. 1977.
3. Fisher, M.J., and Harper Bourne, M., “Source location in jet flows”, Aeronautical Research Council Report ARC 35/383/N910, 1974.

4. Billingsley, J., and Kinns, R., "The acoustic telescope", Journal of Sound and Vibration, Vol. 48, No. 4, pp. 485-510, 1976.
5. Holthusen, H.H.; Smit, H.; A new data acquisition system for microphone array measurements in wind tunnels, AIAA Paper 2001-2169, 2001.
6. Takano, Y.; Horihata, K.; Kaneko, R.; Matsui, Y.; Fujita, H.; Analysis of sound source characteristics of Shinkansen cars by means of X-shaped microphone array, Internoise 96, Liverpool, 1996.
7. Barsikow, B.; Experiences with various configurations of microphone arrays used to locate sound sources on railway trains operated by the DB AG, Journal of Sound and Vibration, Vol. 193, No. 1, 1996, pp. 283-293.
8. Michel, U.; Barsikow, B.; Helbig, J.; Hellmig, M.; Schüttpelz, M.; Flyover noise measurements on landing aircraft with a microphone array, AIAA Paper 98-2336, 1998.
9. Piet, J.-F.; Elias, G.; Localization of acoustic source from a landing aircraft with a microphone array, AIAA Paper 99-1811, 1999.
10. Barsikow, B.; King III, W.F.; On removing the Doppler frequency shift from array measurements of railway noise, Journal of Sound and Vibration, Vol. 120, No. 1, 1988, pp. 190-196.
11. Howell, G.P.; Bradley, A.J.; McCormick, M.A.; Brown, J.D.; De-Dopplerization and acoustic imaging of aircraft fly-over noise measurements, Journal of Sound and Vibration, Vol. 105, No. 1, 1986, pp. 151-167.
12. Sijtsma, P.; Oerlemans S.; Holthusen, H.H.; Location of rotating sources by phased array measurements, AIAA Paper 2001-2167, NLR-TP-2001-135, 2001.
13. Johnson, D.H.; Dudgeon, D.E.; Array Signal Processing, Prentice Hall, 1993.
14. Williams, E.G.; Fourier Acoustics, Academic Press, 1999.
15. Press, W.H.; Teukolski, S.A.; Vetterling, W.T.; Flannery, B.P.; Numerical Recipes, Cambridge, 1994.
16. Lynn, P.A.; Fuerst, W.; Introductory Digital Signal Processing with Computer Applications, Wiley, 1998.
17. Lighthill, M.J.; Introduction to Fourier Analysis and Generalised Functions, Cambridge, 1978.
18. Harris, F.J.; On the use of windows for harmonic analysis with the discrete Fourier transform, Proceedings of the IEEE, Vol. 66, No. 1, 1978, pp. 51-83.
19. Mueller, T.J. (Ed.); Aeroacoustic Measurements, Springer, 2002.
20. Underbrink, J.R.; Dougherty, R.P.; Array design of non-intrusive measurement of noise sources, Noise-Con 96, Seattle, Washington, 29 September-2 October 1996.
21. Sijtsma, P.; Optimum arrangements in a planar microphone array, Presented at the First CEAS-ASC Workshop: Wind Tunnel Testing in Aeroacoustics, DNW, 5/6 November 1997.

22. Abramowitz, M.; Stegun, I.A. (Eds.); Handbook of Mathematical Functions, Dover Publ., 1970.
23. Press, W.H.; Teukolski, S.A.; Vetterling, W.T.; Flannery, B.P.; Numerical Recipes, Cambridge, 1994.
24. Dougherty, R.P.; Turbulent decorrelation of aeroacoustic phased arrays: Lessons from atmospheric science and astronomy, AIAA Paper 2003-3200, 2003.
25. Daigle, G.A.; Piercy, J.E.; Embleton, T.F.W.; Line-of-sight propagation through atmospheric turbulence near the ground, Journal of the Acoustical Society of America, Vol. 74, No. 5, 1983, pp. 1505-1513.
26. Tatarski, V.I.; The effects of the turbulent atmosphere on wave propagation, Israel Program for Scientific Translations, Jerusalem, 1971.
27. Tatarski, V.I.; Wave Propagation in a Turbulent Medium, McGraw-Hill, 1961.
28. Sijtsma, P.; Wal, H.M.M. van der; Identification of noise sources on civil aircraft in approach using a phased array of microphones, NATO symposium SET-079 “Capabilities of Acoustics in Air-Ground and Maritime Reconnaissance, Target Classification and - Identification”, Lerici, Italy, 26-28 April 2004.
29. Dougherty, R.P.; Source location with sparse acoustic arrays; interference cancellation, Presented at the First CEAS-ASC Workshop: Wind Tunnel Testing in Aeroacoustics, DNW, 5/6 November 1997.
30. Sijtsma, P.; Holthusen, H.H.; Source location by phased measurements in closed wind tunnel test sections, AIAA Paper 99-1814, NLR-TP-99108, 1999.
31. Wal, H.M.M. van der; Sijtsma, P.; Flap noise measurements in a closed wind tunnel with a phased array, AIAA Paper 2001-2170, NLR-TP-2001-632, 2001.
32. Cox, H.; Zeskind, R.M.; Owen, M.M.; Robust Adaptive Beamforming, IEEE Proceed-ings on Acoustics, Speech and Signal Processing, Vol. ASSP-35, No. 10, 1987, pp. 1365-1376.
33. Brooks, T.F.; Humphreys Jr., W.M.; Effect of directional array size on the measurement of airframe noise components, AIAA Paper 99-1958, 1999.
34. Howe, M.S.; Acoustics of Fluid-Structure Interactions, Cambridge University Press, 1998.
35. Dowling, A.P.; Ffowcs Williams, J.E.; Sound and Sources of Sound, Wiley, 1983.
36. Treves, F.; Basic Partial Differential Equations, Academic Press, 1975.
37. Oerlemans, S.; Schepers, J.G.; Guidati, G.; Wagner, S.; Experimental demonstration of wind turbine noise reduction through optimized airfoil shape and serrations, Proceedings of the European Wind Energy Conference and Exhibition, Copenhagen, 2-6 July 2001, NLR-TP-2001-324, 2001.